Nanoscale Advances

ROYAL SOCIETY OF CHEMISTRY

PAPER

View Article Online
View Journal | View Issue

Cite this: *Nanoscale Adv.*, 2026, **8**, 2291

Electrocatalytic activity of MoP/CNTs nanohybrid for water splitting: a step towards improved HER kinetics

Ayesha Rehman,[a] Erum Pervaiz, *[ab] Zirwa Noor[a] and Waheed Miran[a]

For a successful shift to sustainable hydrogen evolution catalysis, high-performance electrocatalysts that are both active and stable without the use of precious metals are required. In the case presented within this study, a pure phase molybdenum phosphide–carbon nanotubes (MoP/CNTs) nanohybrid is introduced as a bidirectional electrocatalyst for alkaline water splitting. In the MoP/CNTs nanohybrid, the MoP shows superior catalytic performance with low overpotentials of 81 mV for the hydrogen evolution reaction (HER) and 245 mV for the oxygen evolution reaction (OER), with Tafel slopes of 34 mV dec^{-1} and 96 mV dec^{-1}, respectively. The MoP/CNTs nanohybrid is capable of overall water splitting with high efficiency *via* the formation of an electronic interface between the MoP active sites and the conductive CNTs support. Phosphide–carbon nanohybrids can now be employed as an abundant resource approach for the sustainable evolution of hydrogen.

Received 19th January 2026
Accepted 10th February 2026

DOI: 10.1039/d6na00046k

rsc.li/nanoscale-advances

1. Introduction

The growing need for eco-friendly energy technologies has made the world's efforts to make hydrogen that doesn't add to climate change even stronger. Hydrogen is widely seen as a next-generation energy carrier because it has a high gravimetric energy density, doesn't release any carbon when used, and can be used with large-scale energy storage and transport systems.[1] Among all available methods of hydrogen production, the electrochemical water-splitting process is one of the strategically important technologies due to its high efficiency, operational scalability, and perfect match with renewable, intermittent solar and wind power.[2–4] Notwithstanding the elegance of its underlying mechanism, a symmetry problem has existed in the actual process of water electrolysis in that the reaction rate for both the oxygen evolution reaction (OER) and the hydrogen evolution reaction (HER) has been kinetically sluggish. To overcome this, a high potential is required, but this is invariably accompanied by losses in efficiency and remote economies of scale for scaling up the process. To date, the highest performing electrolyzer cells still use platinum for the HER and ruthenium or iridium oxides for the OER, but due to their availability and long-term stability, these precious metals still tend to pose a severe challenge for scaling up.[5]

In this regard, onset metal-based electrocatalysts have been identified as promising substitutes for noble metals, and in this category, TMPs have garnered keen interest. TMPs possess inherent metallicity, desirable hydrogen adsorption enthalpies, and enhanced charge transfer rates, which are desirable in an HER catalyst.[6,7] Under these conditions, the co-existence of metal and phosphorus points within these materials as hydride acceptor and proton acceptor sites offers a synergetic catalytic environment.[8–10] Of all the TMP compounds, molybdenum phosphide, denoted as MoP, has been gaining popularity owing to its high electrical conductivity, chemical robustness, and economical feasibility.[11,12] The presence of phosphorus, which has a low ionization energy and utilizes vacant 3p orbitals and a pair of lone-electron pairs, leads to localized charge density and facilitates proton trapping, thus promoting kinetics in the HER process.[12–14] Promising results for the performances of HER and bifunctional water splitting have been achieved for the phosphide materials, namely cobalt phosphides and nano-MoP catalysts. In particular, orthorhombic-CoP and Co_2P have been able to show stable catalysis during prolonged periods of usage, and the nanostructure and amorphous nature of MoP improve the overall performance of the material compared with bulk counterparts by suppressing the hydrogen binding energy and providing an increased number of accessible active sites.[15] Nonetheless, these achievements have revealed inherent challenges. For instance, the preparation of high-quality MoP with good crystal structure usually requires high-temperature treatment (>700 °C), which is likely to cause particle agglomeration and inhomogeneous phase distribution. In addition, the

[a]*Heterogeneous Catalysis Lab, Department of Chemical Engineering, School of Chemical and Material Engineering (SCME), National University of Sciences and Technology (NUST), Islamabad, 44000, Pakistan. E-mail: erum.pervaiz@scme.nust.edu.pk*

[b]*Laboratory for Chemical Technology (LCT), Department of Materials, Textiles and Chemical Engineering, Faculty of Engineering & Architecture, Gent University, 9052, Gent, Belgium*

multistep synthesis method is likely to raise the fabrication cost and difficulties. Research efforts in bimetallic or heterostructural systems aiming at addressing these challenges have shown improved local performance but face challenges of instability or low durability.[5,16]

However, these restrictions indicate an important knowledge gap: high catalytic activity does not guarantee functioning without adequate integrity and functional architecture in relation to catalyst supports. Carbonaceous supports have been shown effective for enhancing electronic conductivity, although it has also been a poorly explored area in relation to understanding the significance of interactions in suppressing volume expansion and performance-related restrictions of the catalyst. Of the conductive supports, carbon nanotubes (CNTs) have shown remarkable strength, high surface area, and good chemical and thermal stability, with conductivity in the range of 10^4 S cm^{-1}, making them excellent supports for preparing phosphide catalysts.[10,17,18] In this study, we demonstrate an MoP/CNTs microsphere architecture that targets the activity–stability dilemma in HER electrocatalysts with simplicity in material complexity rather than complexity in composition. The rationale for employing MoP/CNTs nanohybrids in this study is founded on their complementary properties in catalysis, where MoP possesses high catalytic active site density and CNTs serve as a conductive support that ensures optimal electron transfer between the catalytically active material and the electrode surface. By incorporating MoP nanoparticles in an interconnected CNTs network that utilizes a simple solid-state processing method, nanoparticle clustering, volume change, and electrode material stability are prevented even during sustained electrochemical tests.[19] Notably, this research proves that the electrocatalytic properties of MoP/CNTs hybrids are dominantly impacted by CNTs loading, as higher loading of carbon may impede access to active sites, while properly mixed CNT loading promotes maximum utilization of Mo–P active sites. This microspherical morphology allows for maximal exposure of active sites and facilitates charge transport and toughness.[20] Furthermore, in addition to reaching a competitive HER performance level that can rival that of benchmark Pt/C electrocatalysts, it provides a clear and rational framework for designing electrocatalysts based on abundant materials, with emphasis on structural stability and scalability and, by extension, robustness and longevity.[21,22] Rather than emphasizing metrics for isolable performance, it proposes a clear direction towards achieving economical and scalable hydrogen production methods.[23]

2. Experimental study

2.1 Chemicals and materials used

Sodium hypophosphite monohydrate ($NaH_2PO_2 \cdot H_2O$), sodium molybdate dihydrate ($Na_2MoO_4 \cdot 2H_2O$), sulfuric acid (H_2SO_4), and nitric acid (HNO_3) were purchased from Sigma-Aldrich. Ethanol (≥99.9%) and methanol (grade quality) were obtained from Merck. During electrochemical measurement nickel foam (thickness: 1.5 mm, area: 1 × 1 cm) served as the substrate for catalyst deposition. In the catalyst ink, PVDF solution was employed as a binder. The calcination was carried out in an inert atmosphere with 99.999% pure Ar gas. All solution preparations used DI water.

2.2 Activation of carbon nanotubes (CNTs)

In a typical procedure, 1 g of multi-walled carbon nanotubes (MWCNTs) was dispersed in a mixed acid solution containing concentrated sulfuric acid (98%, 18.75 mL) and nitric acid (68%, 6.25 mL) in a 100 mL round-bottom flask. The suspension was refluxed at 80 °C for 3 h under continuous stirring to introduce surface functional groups. The resulting black solid was collected by centrifugation, thoroughly washed with deionized water several times until neutral pH was achieved, and subsequently dried at 70 °C for 24 h. The acid-treated material is hereafter referred to as functionalized MWCNTs.[24]

2.3 Synthesis of MoP electrocatalyst

MoP was synthesized *via* a solid-state synthesis method. For a typical synthesis, 300 mg of sodium molybdate dihydrate ($Na_2MoO_4 \cdot 2H_2O$) was mixed with 3 g of sodium hypophosphite monohydrate ($NaH_2PO_2 \cdot H_2O$) and ground thoroughly using a mortar and pestle for approximately 30 minutes. Thereafter, the uniform precursor mixture was transferred into a ceramic boat and calcined for two hours at 750 °C while being continuously exposed to argon gas. The final product was centrifuged and dried overnight at 70 °C after spontaneously cooling to room temperature and being repeatedly cleaned (five washing cycles) with deionized water.[25]

2.4 Synthesis of MoP/CNTs hybrid electrocatalysts

MoP/CNTs hybrids were synthesized by incorporating CNTs into a $Na_2MoO_4 \cdot 2H_2O$ and $NaH_2PO_2 \cdot H_2O$ precursor mixture. A schematic representation of the synthesis procedure is shown in Fig. 1. For the purpose of achieving homogeneity, the reactants were crushed together for 30 minutes using a mortar and pestle. The resultant homogenous mixture was then placed in a ceramic boat and subjected to a heating rate of 10 °C per minute for a period of two hours at a temperature of 750 °C in an Ar atmosphere. The addition of CNTs in the synthesis of MoP nanoparticles was significant in resisting the agglomeration/sintering processes that occurred as a result of the high temperature interactions between the metal and the CNTs.

Then, the final product was centrifuged and washed repeatedly using deionized water and dried at 70 °C overnight. The concentration of CNTs was changed in order to synthesize MoP/CNTs hybrids with different CNTs composition.

2.5 Preparation of working electrode

Catalyst ink was prepared and then coated on a pre-treated nickel foam to develop the functional electrode. The nickel foam substrate was cleaned with ethanol and HCl before use. The catalyst ink was produced from 5 mg of carbon black, 2.5 mg of PVDF binder, 42.5 mg of the synthesized catalyst, and 0.3–0.4 mL of *N*-methyl-2-pyrrolidone (NMP) as solvent. The sonication of the mixture was conducted in an ultrasonication

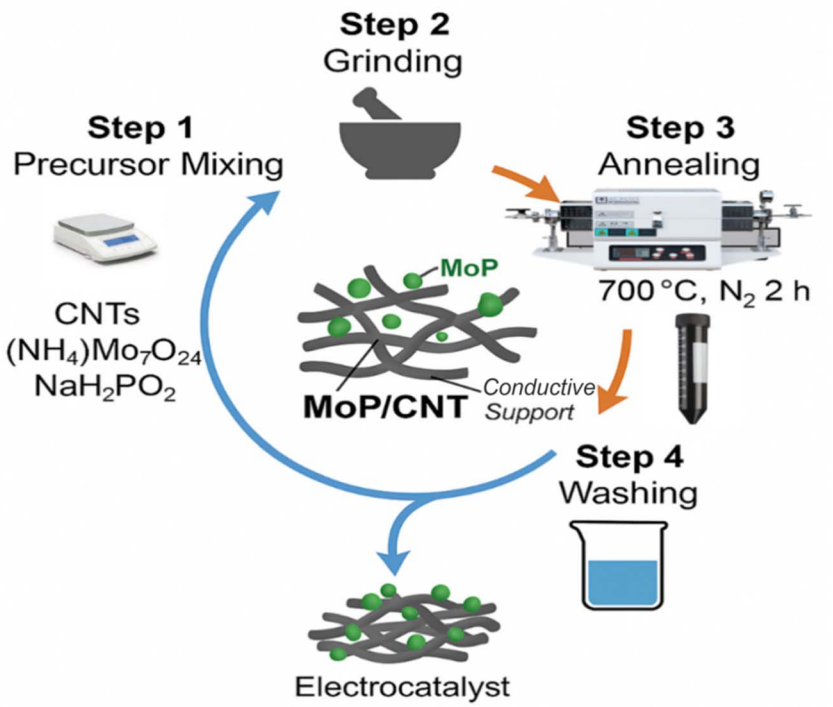

Fig. 1 Process flow diagram of MoP/CNTs hybrids synthesis.

bath for four hours to ensure uniform dispersion. After sonication, the ink was evenly spread over the nickel foam, compressed at a pressure of 1 bar to enhance the adhesion, and dried overnight at 80 °C to obtain the final electrode.

3. Material characterization

The XRD (STOE-SEIFERT XPERT PRO) analysis was done using Cu Kα radiation from 0° to 90° degrees in an attempt to identify the composition and formation of phases. Energy-dispersive X-ray analysis, carried out using scanning electron microcopy (SEM, model: JSM6490A, available from the Japan-based company JEOL), was utilized in an attempt to determine the shape and composition of catalyst surfaces. In an attempt to establish the average size of the MoP and CNTs hybrids, Scherrer's equation (eqn (1)) was used:

$$D = \frac{k\lambda}{\beta \cos \theta} \quad (1)$$

D is the crystallite size, K is Scherrer's constant, which has a value of 0.9 (shape factor), θ is the full width at half maximum, Θ is the Bragg angle, and D is the X-ray wavelength, which has a value of 0.15406 nm.

3.1 Electrochemical testing

Electrocatalytic performance of the as-synthesized MoP/CNTs catalysts for HER was measured by an Origa Lys instrument (Model 5) with a conventional three-electrode. Platinum wire served as the counter electrode, catalyst-coated nickel form as the working electrode, and an Ag/AgCl electrode as the reference electrode. An aqueous solution of 1 M KOH was utilized as the electrolyte. All measured potentials were converted to the reversible hydrogen electrode (RHE) scale for comparison.

Nernst equation that is applied.

$$E_{Ag/AgCl} + (0.059 \times pH) + E_{0,Ag/AgCl} = E_{RHE} \quad (2)$$

$E_{Ag/AgCl}$ is 0.1976 and pH is 14 in the provided eqn (2).

Electrochemical impedance spectroscopy (EIS), linear sweep voltammetry (LSV), cyclic voltammetry (CV), and chronopotentiometry were used to evaluate the electrochemical performance of the synthesized catalysts. The Tafel slopes, acquired from eqn (3) of the Tafel equation, are invaluable indicators of catalytic effectiveness and reaction kinematics of the HER process.[26]

$$\eta = b \log j + \alpha \quad (3)$$

An assessment of turnover frequency (TOF) was determined using eqn (4).

$$\mathrm{TOF} = \frac{j \times A}{\alpha \times f \times n} \quad (4)$$

Here, A represents the electrode surface area, the Faraday constant is represented by F, the current density by j, and the number of electrons transported by α, which varies for HER and OER processes. On the basis of chrono–potentiometric analysis, the stability of electrocatalysts was estimated. EIS analysis was also carried out over an extensive range of frequencies from 100 kHz to 0.1 Hz, along with a low amplitude of the AC probe of 10 mV. This facilitates estimation of electrochemical capacitance based on eqn (5).

$$C_p = \frac{A}{(2 \times m \times k) \times (V_2 - V_1)} \quad (5)$$

Here, A is the surface area difference between the surface area calculated from the CV graph and the CV curve. m is the mass of the loaded catalyst in grams (g), and k is the speed at which the catalyst accomplished its cycle. $(V_2 - V_1)$ = defined as the potential window (V) available in the system for the operation of the catalyst. Eqn (6) and (7) are employed in determining the performance parameters.

$$\mathrm{ECSA} = \frac{C_{dl}}{C_s} \quad (6)$$

$$C_{dl} = \frac{(Y_o \times R_p)^{1/\alpha}}{R_p} \quad (7)$$

C_s: specific capacitance unit is F cm^{-2}, C_{dl}: double layer capacitance unit is farad.

4. Results and discussion

4.1 Analysis of phase morphology and functional groups

In Fig. 2, analysis of the crystal and chemical structures of MoP and MoP/CNTs hybrid structures reveals significant information regarding phase purity, interface coupling, and structural stability parameters, which are crucial for electrocatalysis. The X-ray diffraction (XRD) pattern of pristine MoP Fig. 2a(i) exhibits well-defined reflections at $2\theta = 27.41°$, 31.57°, 42.53°, and 46.21°, corresponding to the (001), (100), (101), and (110) planes of hexagonal MoP (JCPDS No. 03-065-6024).[20] Such reflections prove the successful synthesis of single-phase MoP with a hexagonal crystal structure and the space group $P6m2$, in which Mo atoms have been six-coordinated with phosphorus atoms. Worth noting is that this coordination geometry is very similar to that of platinum metal, and this explains the reason why platinum metal-like catalytic activity often exists in MoP-based HER.

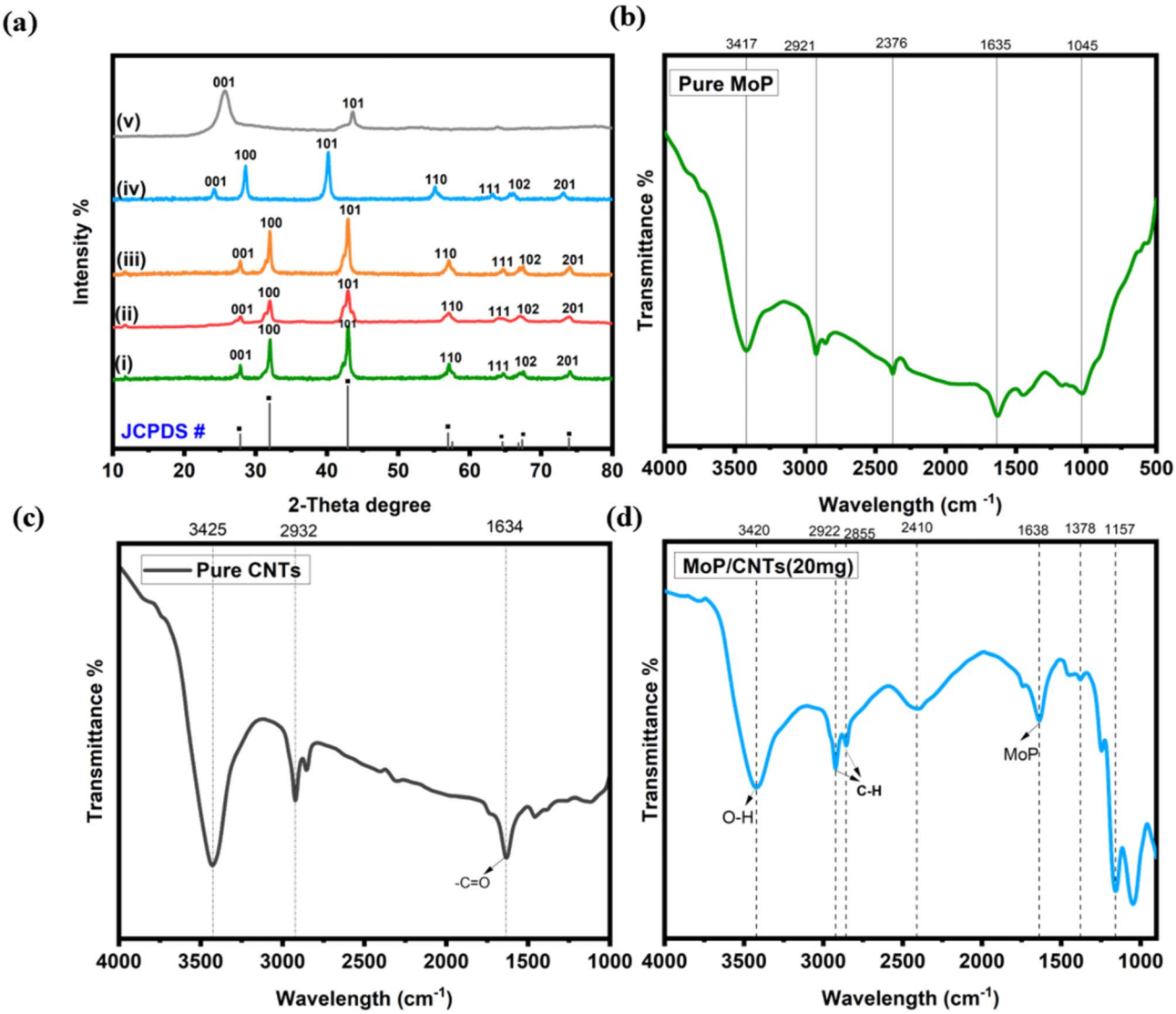

Fig. 2 (a) (i) Pure MoP, (ii, iii and iv) MoP/CNTs (10 mg), (15 mg), (20 mg), (v) pure CNTs. (b) FTIR curve for pure MoP. (c) FTIR curve for CNTs, (d) MoP/CNTs (20 mg).

Fig. 2a(v) Diffraction pattern of CNTs matches very well with standard reference (JCPDS No. 00-058-1638) indicating the sound structure of the material even after synthesis and processing. Notably, the MoP/CNT hybrid samples containing different amounts of CNTs (10 mg, 15 mg, and 20 mg) Fig. 2a(ii, iii and iv) exhibit the characteristic diffraction peaks of MoP without the evolution of any secondary phases, thereby confirming that the presence of CNTs does not disturb the crystallization of MoP. For all hybrid samples, the (101) plane is found to be the dominant peak at 42.54°. Minor changes in the peaks and slight expansion in the lattice are observed, which can be credited to the strains caused by the interface between MoP/CNTs, rather than a phase transformation, and this is an important strength of CNTs dispersion, where it adds flexibility to the crystallographic structure.[18] An examination of the crystallite size calculations made by Scherrer's Equation indicates a gradual reduction in the MoP crystallite size with increased CNTs loading, from 65.77 nm to 48.38 nm as shown in Table 1. This size modulation reflects the role of CNTs as spatial confinement scaffolds that suppress high-temperature particle coalescence, a well-known failure mode in phosphide synthesis. Such controlled crystallite refinement is particularly significant because excessive grain growth in MoP has been directly linked to reduced active-site accessibility and rapid performance degradation under electrochemical cycling. Beyond phase identification, FTIR spectroscopy provides molecular-level evidence of interfacial coupling between MoP and CNTs. As shown in Fig. 2(b) FTIR spectrum of pure MoP shows a broad absorption band around 3417 cm^{-1}, which is attributed to –OH stretching vibrations from surface hydroxyl groups or adsorbed moisture. The weak band near 1635 cm^{-1} corresponds to H–O–H bending vibrations. In the low wavenumber region 1045 cm^{-1} characteristic Mo–P vibrational modes are observed, confirming the formation of molybdenum phosphide. In Fig. 2(c) CNTs display expected features corresponding to O–H stretching 3425 cm^{-1}, C–H stretching 2932 cm^{-1}, and graphitic C=C skeletal vibrations 1634 cm^{-1}, indicating retained structural integrity. Notably, the increased intensity of Mo–P vibrational bands in MoP/CNT hybrids suggests enhanced MoP–CNTs interaction and improved dispersion of MoP domains within the conductive network.[27] A key observation is the attenuation of the broad O–H stretching band 3420 cm^{-1} in the MoP/CNTs hybrids compared to pristine MoP. The C–H stretching vibrations near 2922 cm^{-1} and the C=C vibrations around 1638 cm^{-1} confirm the presence of CNTs in the hybrid shown in Fig. 2 (d).

Importantly, the characteristic Mo–P vibration in the 1157 cm^{-1} region is retained, confirming that the MoP crystal structure remains intact after hybridization. This implies decreased surface hydroxyl coverage or modified surface adsorption behavior, which may facilitate faster proton transfer kinetics and reduced parasitic adsorption during HER. Such interfacial chemical modulation is particularly relevant for long-term electrocatalytic stability, where surface hydroxyl accumulation is known to contribute to catalyst passivation.[28] Crucially, post-electrolysis XRD analysis of used MoP/CNTs electrodes reveals no discernible structural degradation or phase evolution, with diffraction profiles remaining nearly identical to those of the pristine samples (SI Fig. S1 and S2). The fact that the MoP peaks are present along with a low background intensity from CNTs and Ni foam indicates a highly stable material structure. This is particularly important for MoP electrocatalysts, where material failure originates from crystal collapse and phase oxidation.

4.2 Morphological analysis of synthesized sample

Morphological development in pristine MoP and hybrid MoP/CNTs structures was analyzed through SEM studies to gain insights into structural properties in terms of catalytic performance, durability, and scalability. From Fig. 3(a), it can be analyzed that pristine MoP consists of tight and dense porous clusters. Although it is advisable to observe tight clusters in MoP materials, it is an issue to be considered seriously because tight assemblies diminish accessibility of electrolytes, which are responsible for lowering active sites along with accelerating degradation in performance during EC studies.[29] In contrast, the original CNTs, Fig. 3(b), exhibit the characteristic and expected entangled tubular structure and high aspect ratio and porosity, aligning well within their established use within strong and conductive structural roles. When MoP is added to CNTs, there is an expected and drastic change in the surface topography, Fig. 3(c), (d), and (e). Over a loading range of 10, 15, and 20 mg, MoP/CNTs hybrids show a hierarchical and interconnected void structure, where the MoP nanoparticles are

Table 1 Crystallite size of prepared electro-catalyst

Catalyst	FWHM	Peak position (2θ)	Crystallite size (nm)	Crystallite size (nm)
Pure MoP	0.182, 0.25	27.41236, 31.57	78.41, 56.50	65.77
	0.328, 0.182	42.5397, 46.216	45.36, 82.82	
Pure CNTs	0.874, 0.218	25.683, 43.260	16.27, 68.42	55.49
	0.218	77.921	81.79	
MoP/CNTs (10 mg)	0.328, 0.291	31.875, 31.875	43.962, 49.552	51.46
	0.291, 0.255	42.875, 54.412	51.18, 61.13	
MoP/CNTs (15 mg)	0.301, 0.301	22.026, 27.912	46.928, 47.465	50.47
	0.328, 0.234	31.435, 43.474	43.924, 63.571	
MoP/CNTs (20 mg)	0.218, 0.328	21.649, 31.804	64.755, 43.954	48.38
	0.328, 0.364	31.806, 42.619	43.954, 40.887	

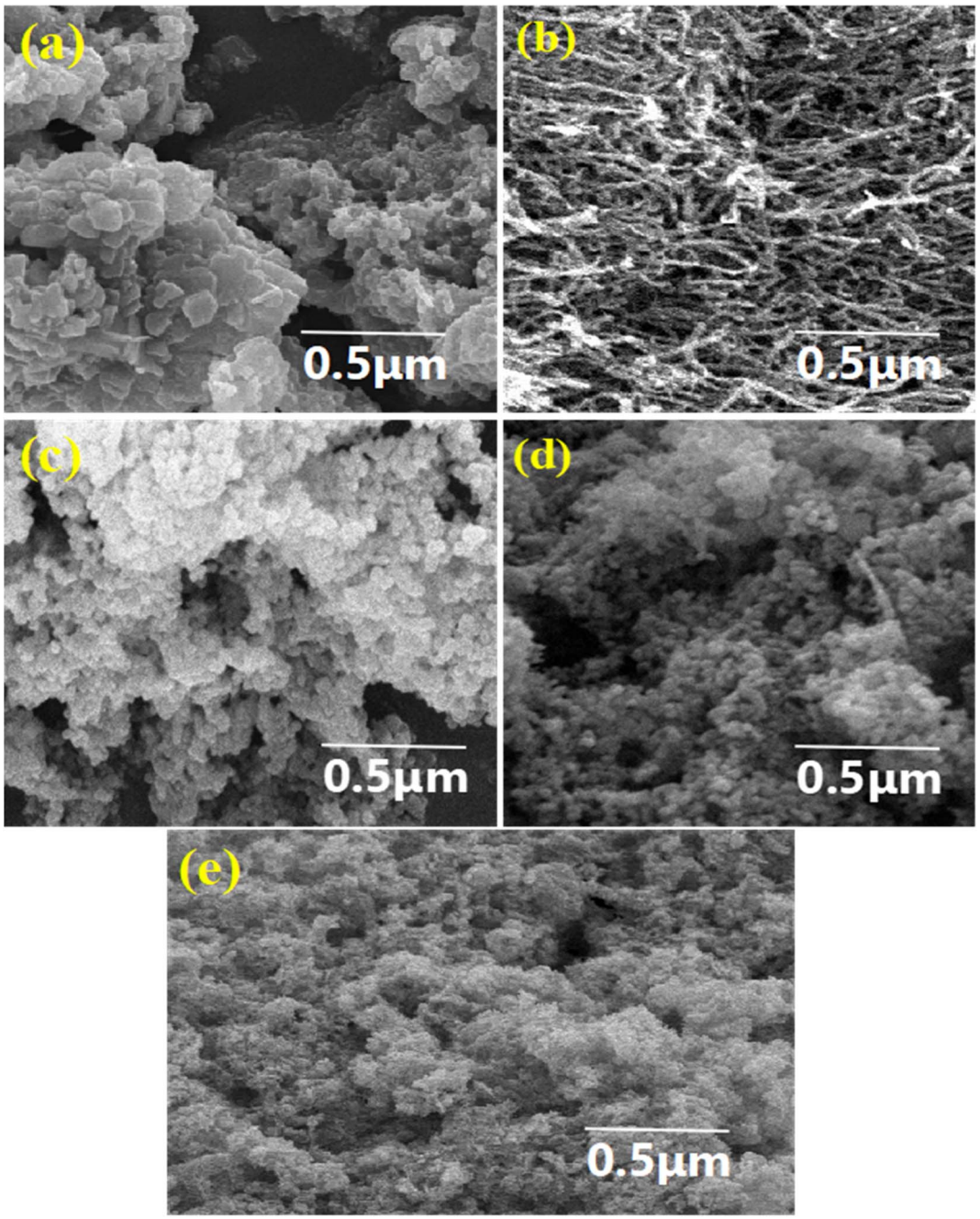

Fig. 3 (a) SEM images of pure sample, (b) pure CNTs, (c–e) hybrids MoP/CNTs.

homogeneously dispersed on the CNTs interfaces, giving a nanorod and roughed appearance. This arrangement is efficient in preventing the agglomeration of MoP nanoparticles and at the same time providing a continuous route for electronic conduction, which has been a challenge in phosphide catalyst materials for a considerable time. It is important to note that increased amounts of CNTs loading lead to rougher surface topography, which is not devoid of void space within the structure. Such inherent structural openness is critical to supporting quick electrolyte diffusion, preventing concentration polarization, and ensuring efficient transport of reactants and products in the hydrogen evolution process. Indeed, the above points emphasize the importance of CNTs loading in hydrogen evolution as more than just a conductivity enhancer, as CNTs serve as spatially separate agents involved in controlling the nucleation and growth of MoP, thus avoiding structural degradation. Such high morphological sensitivity to CNTs loading, in fact, implies CNTs–MoP interaction beyond just the mixture.[30] Energy-dispersive X-ray spectroscopy confirms the elemental composition of MoP and the hybrids Fig. 4, showing a composition of 54.7% Mo and 25.4% P for pristine MoP, as expected. For MoP/CNTs (20 mg) hybrids, peaks for Mo, C, and P are

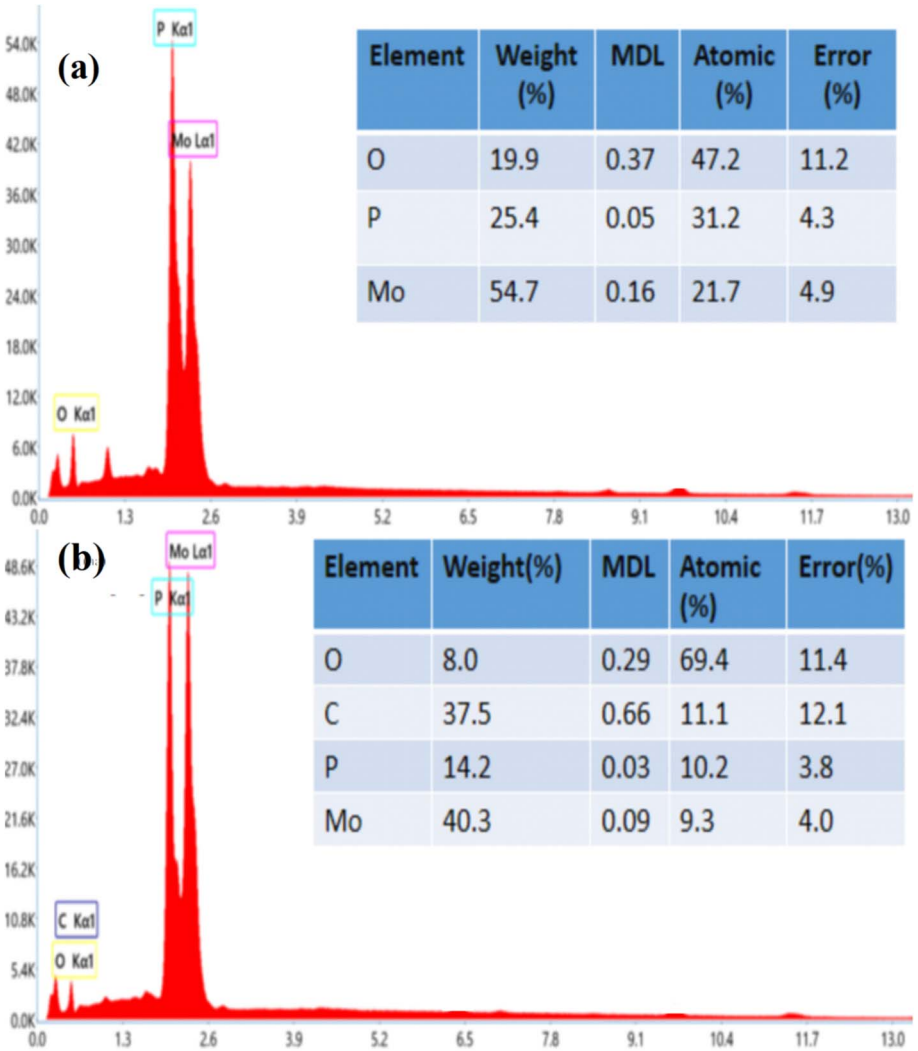

Element	Weight (%)	MDL	Atomic (%)	Error (%)
O	19.9	0.37	47.2	11.2
P	25.4	0.05	31.2	4.3
Mo	54.7	0.16	21.7	4.9

Element	Weight(%)	MDL	Atomic (%)	Error(%)
O	8.0	0.29	69.4	11.4
C	37.5	0.66	11.1	12.1
P	14.2	0.03	10.2	3.8
Mo	40.3	0.09	9.3	4.0

Fig. 4 Elemental composition analysis *via* energy-dispersive X-ray spectroscopy (EDX) (a) MoP, (b) MoP/CNTs 20 mg.

identified, with a corresponding composition of 40.3% Mo, 37.5% C, and 14.2% P, respectively. This high C content confirms the incorporation of CNTs into MoP, supporting the structural analysis obtained from SEM images.[31] To assess the applicability of this architecture as a means of device-scale functionality, the MoP/CNTs hybrid material was deposited as an electrode and the resultant electrode morphology is presented in Fig. S3 and S4. On the whole, the hybrid material exhibits an excellent conformal coverage of the entire three-dimensional porous architecture of the Ni foam. This is an imperative requirement that provides a uniform pathway for the electrons from the current collector as well as enables the diffusion of the electrolyte.

4.3 Electro-chemical study of pure sample and hybrids

The electro-chemical properties of bare MoP and MoP/CNTs hybrid catalysts have been explored using cyclic voltammetry (CV), to understand charge transfer mechanisms, redox accessibility, and inherent catalytic activity. As depicted in Fig. 5(a), addition of CNTs to MoP has increased electro-chemical activity substantially. The addition of CNTs to MoP has helped to sustain efficient charge transfer between redox sites, in addition to facilitating ion diffusion within a porous electro-chemical cell. This is an important aspect because MoP catalysts have often exhibited limitations due to potential electronic bottlenecks.

To gain deeper insights into the redox kinetics and charge storage property of the sample, CV curves of MoP/CNTs (20 mg) were recorded at scan rates from 5 mV s^{-1} to 100 mV s^{-1} as shown in Fig. 5(b). Well-resolved pairs of redox peaks are recorded in the potential range of 0–0.6 V, confirming the reversible nature of the electrochemical reactions involving the surface accessible MoP catalytic sites. What is remarkable is the independence of the CV cycle with scan rate, indicating low inherent resistance and fast mass transport characteristics that are desirable qualities for an electrochemical material.[32] The progressive enhancement of redox peak currents with the scan rate is an additional confirmation of the surface-limited nature of the electrochemical process of the MoP/CNTs hybrid. Such a surface-limited process is a result of the CNTs support, which

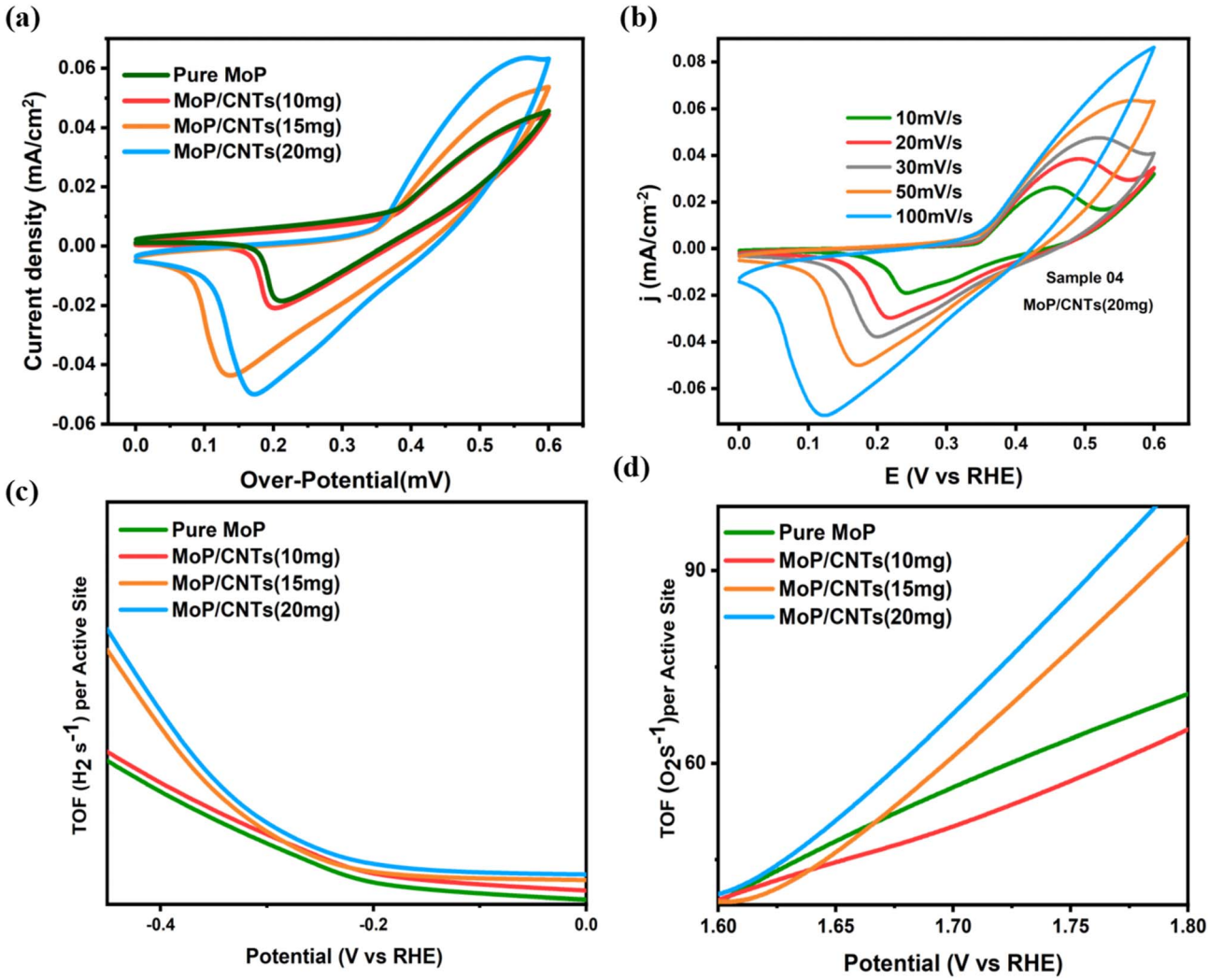

Fig. 5 (a) CV for all samples; (b) MoP/CNTs (20 mg) at different scan rates (c and d) TOF for HER and OER.

not only prevents the MoP nanoparticles from clustering but also provides a path for the passage of electrons with each cycle. The MoP structure in a hexagonal morphology within the carbon matrix is a major reason for the availability of the redox sites and the quick passage of electrons along with the prevention of degradation.[33] Apart from the qualitative electrochemical fingerprints, the inherent catalytic property was evaluated on the basis of turnover frequency (TOF) calculated for both HER and OER as shown in Fig. 5(c) and (d). TOF values increase systematically with the addition of CNTs, and MoP/CNTs (20 mg) have the highest inherent catalysis amongst all the samples examined. The improved catalysis cannot be solely ascribed to the enhanced surface area and instead relate to the modification of the electronic property inside the MoP/CNTs interface.

The bifunctionality of pure MoP, CNTs, and MoP/CNTs hybrids was investigated systematically in a 1.0 M KOH electrolyte in an effort to understand the role of interface engineering for hydrogen and oxygen evolution. As indicated in Fig. 6(a) and (b), each MoP/CNTs hybrid showed a strong reduction in its HER overpotentials compared to its individual component, pointing out the dominant role of MoP and CNTs interface engineering. Under a typical current density of 10 mA cm^{-2}, there is a gradual reduction in overpotentials from 186 mV for 10 mg of CNTs to 141 mV for 15 mg of CNTs, to reach a lowest point of 81 mV for MoP/CNTs of 20 mg, thus highlighting an optimal heterostructural area rather than CNTs-loading phenomena.[34] However, this achievement cannot be attributed solely to the intrinsic conductivity of MoP and the high surface area of CNTs. Instead, it should be attributed to the increased density of MoP/CNTs heterointerfaces, which allow for efficient electronic coupling, facilitate catalytically active MoP edges, and inhibit nanoparticle agglomeration during operation. Although MoP has an electronic structure similar to that of Pt, favoring proton-electron coupling at a wide range of pH values, its standalone use is impeded by low active site accessibility and interelement charge transport. Additionally, the CNTs template eliminates these issues by allowing for efficient, macroscopic-scale electron transport along with the induction of local modifications to the electronic states of Mo

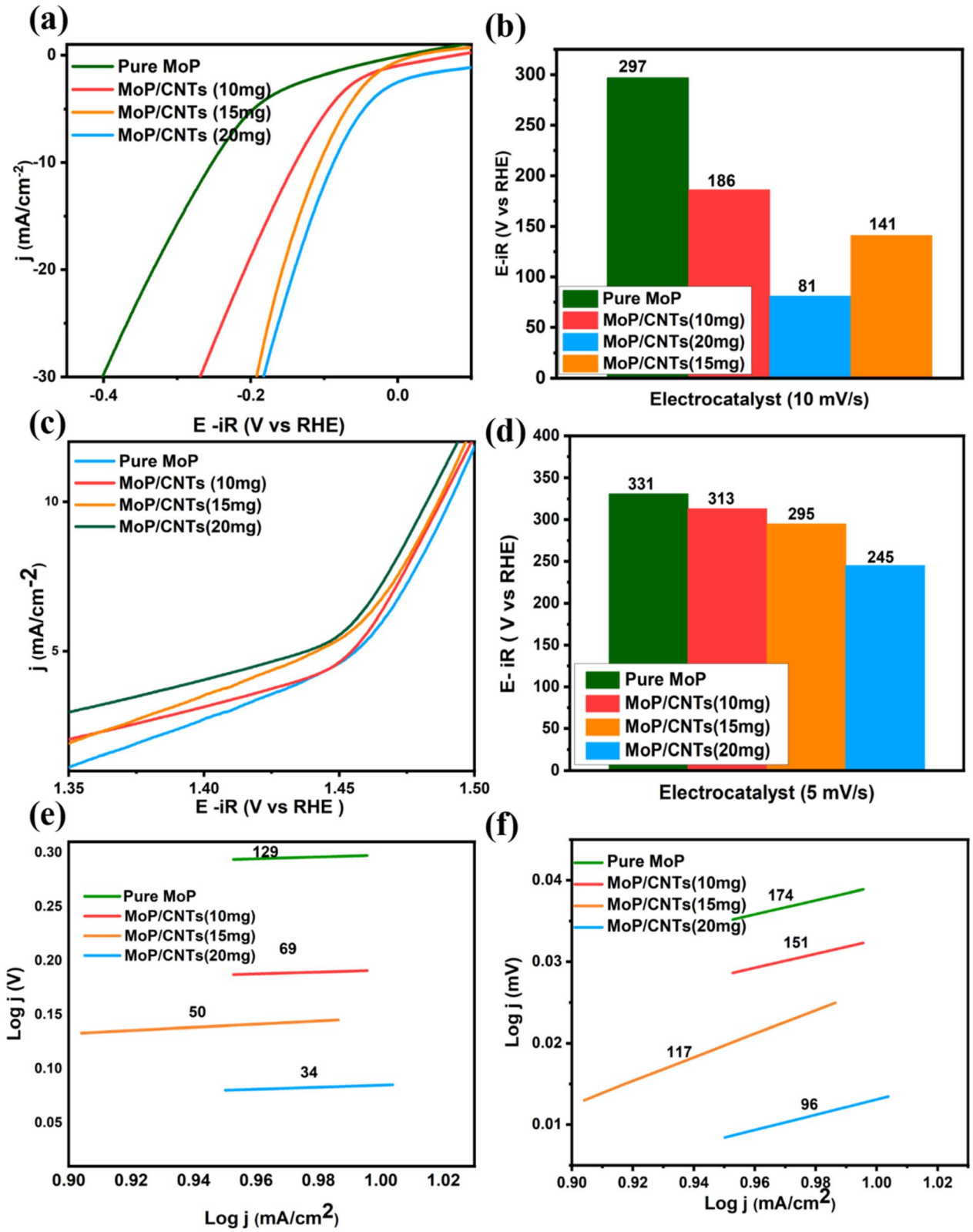

Fig. 6 (a and b) HER potential for MoP and their hybrids. (c and d) OER potential for MoP and their hybrids. (e and f) Tafel slope for HER & OER respectively.

and P. Such a combination facilitates faster proton adsorption and desorption kinetics for hydrogen evolution, favoring a surface-dominated mechanism. In addition to hydrogen evolution, the MoP/CNTs hybrids show considerable activity towards oxygen evolution, qualifying the system to be a true dual-functional electrocatalyst.

It can be observed from Fig. 6(c) and (d) that MoP/CNTs (20 mg) exhibits an OER overpotential of 245 mV at 10 mA cm^{-2}, outperforming pure MoP (295 mV), commercial Pt/C (357 mV), and lower-CNTs-content hybrids. The inferior OER response of Pt/C arises from the formation of inactive surface oxides under anodic conditions, highlighting the fundamental limitation of noble-metal catalysts for alkaline OER. In contrast, the efficient charge transfer is sustained and the structure is maintained in the MoP/CNT architecture, emphasizing the advantages brought about by the transition-metal phosphide–carbon heterostructure toward high-performance alkaline water electrolysis.[35] The kinetic understandings confirmed by Tafel slope analysis further support the excellent mechanism advantage of the optimal hybrid. The Tafel slope for HER with the sample of MoP/CNTs (20 mg) shows the lowest value of 34 mV dec^{-1}, greatly outperforming pure MoP with a Tafel slope of 50 mV dec^{-1} and CNTs-based hybrids, as shown in Fig. 6(e), confirming faster surface charge transfer and easily accessible reaction channels. The Tafel analysis for OER shows that the sample with the lowest Tafel slope of 96 mV dec^{-1} for all assessed electrocatalysts is MoP/CNTs (20 mg), as shown in Fig. 6(f), representing faster reaction rates and optimal active surface engagement. More notably, these benefits are successfully enlarged by combining with conductive nickel foam, contributing to increased structural integrity, reduced internal contact resistances, and maximized exposure of hexagonal surfaces in MoP/CNTs, as illustrated.[36] Despite these advances, the optimization study in fact reveals an important limitation of the current hybrid design strategies. High loadings of CNTs (140–260 mg) result in catastrophic performance degradation SI Fig. S5, displaying high overpotentials coupled with repressed current densities. Such failures arise from CNTs agglomeration that masks active sites of MoP, disrupts the proton diffusion pathway, and compromises the interfacial charge transfer. These observations underscore a persistent challenge in hybrid electrocatalysts: how to maximize conductivity while not sacrificing catalytic accessibility. In this regard, identification of 20 mg CNTs as the optimal composition clearly indicates that the catalytic performance is controlled by the interface architecture rather than the abundance of components. This work advances phosphide–carbon interfacial design but resolving *operando* electronic reconstruction and long-term active-site stability will require *operando* diagnostics, multiscale modeling, and standardized benchmarking. Different electrocatalyst performance for HER and OER has been reported Tables 2 and 3.

EIS provides critical mechanistic insight into why the optimized MoP/CNTs (20 mg) hybrid transcends conventional phosphide-based electrocatalysts. As shown in Fig. 7(a) and (b) the Nyquist response reveals a pronounced contraction of the semicircle diameter, directly evidencing a substantial reduction in charge-transfer resistance and accelerated interfacial kinetics for the OER. "This behavior represents more than a mere increment in conductivity, as it reflects a fully optimized, differently configured electrode/electrolyte interface that would result from rational phosphide carbon coupling." The proximity of the impedance arc to the imaginary axis reflects efficient electron percolation channels as well as rapid ion diffusion, both of which are still problematic within transition metal phosphides, especially within an alkaline environment.[48] Equivalent circuit analysis also serves to further elucidate this performance enhancement. The measured polarization resistance (R_{ct}) thereof is reduced with increasing applied potential, emphasizing this voltage-sensitive behavior of the MoP/CNTs interface. This is in stark contrast to both pristine MoP electrodes where slowed charge accumulation and interface-induced restrictions are prominent at higher current densities.[49] The integration of CNTs thus rectifies the long-standing

Table 2 Comparison of HER potential for different electrocatalyst

Electrocatalyst	Over-potential (mV)	Tafel slope (mV dec^{-1})	Current density (mA cm^{-2})	Stability (h)	Ref.
MoP/CNTs (20 mg)	**81**	**34**	**10**	**24**	**This work**
MoP/CNTs	86	60	10	24	37
MoP@NCF	121.8	72.4	10	30	38
MoP/NG	94	50.1	10	20	39
MoS_2/MoP/CNTs	73	56	10	12	40
CoP/MoP	183	53.3	10	10	41

Table 3 Comparison of different OER potential of electrocatalyst

Electrocatalyst	Over-potential (mv)	Current density (mA cm^{-2})	Tafel slope (mV $dec^{-1)}$	Stability (h)	Ref.
MoP/CNTs (20 mg)	**245**	**10**	**96**	**24**	**This work**
MoP/NiFeP	256	10	31	—	42 and 43
NF/Mn-MoOxSy/NiP	191	10	81.2	10	44
MoP_x@MnP_y	301	20	105	16	45
NMCP@NF	250	10	41	24	46
$Mo_{0.29}Co_{0.71}P_2$/CNTs	220	10	—	12	47

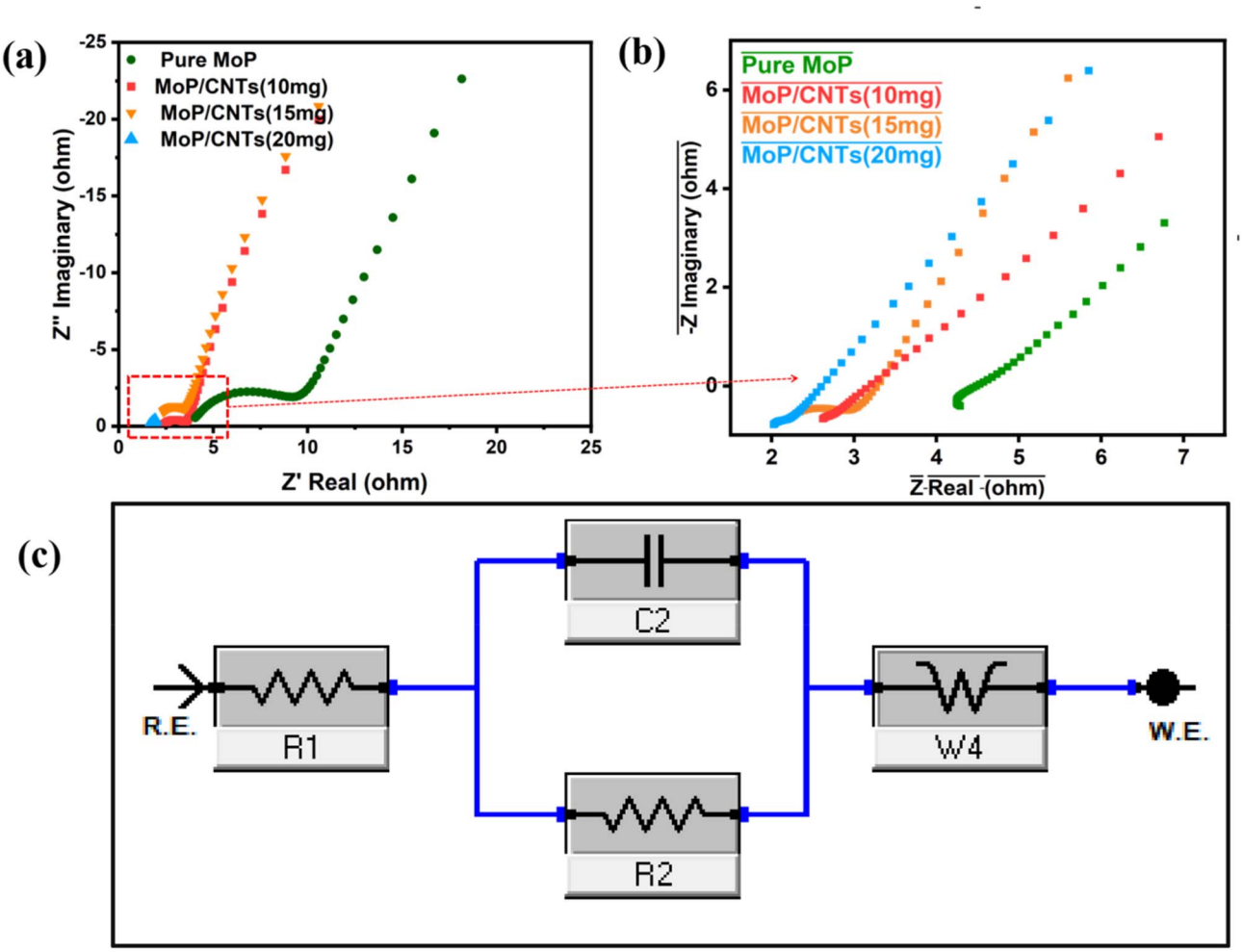

Fig. 7 (a and b) EIS Spectra of prepared electro-catalyst. (c) Equivalent electrical circuit employed for fitting the EIS spectra using Gamry software.

drawback of phosphide catalysts, specifically the decoupling of the inherent catalytic property from overall charge transport under realistic operating conditions.[50] The electrochemical impedance data were analyzed using the equivalent circuit model shown in Fig. 7(c). The circuit comprises a solution resistance (R_1), representing the ohmic resistance of the electrolyte and electrical contacts, connected in series with a parallel combination of a charge transfer resistance (R_2) and a constant phase element (C_2). The CPE accounts for the non-ideal capacitive behavior arising from surface heterogeneity and electrode roughness. Additionally, a Warburg impedance (W_4) element is included to describe ion diffusion processes within the electrolyte and porous electrode structure. This equivalent circuit effectively captures the charge transfer kinetics, interfacial capacitance, and mass transport characteristics of the electrocatalytic system.

Quantification of the ECSA provides additional insight into the structure–activity relationship. Conventional CV-based C_{dl} extraction becomes unreliable for redox-active materials such as MoP/CNTs hybrids due to overlapping faradaic contributions. In this case, CNTs make use of the constant phase element (CPE) fitting approach from electrochemical impedance spectroscopy (EIS) measurements to yield a more accurate and realistic values of C_{dl}. Based on a standardized specific capacitance ($C_s = 40$ μF cm^{-2}) in an alkaline electrolyte solution, the MoP/CNTs (20 mg) hybrid displays an unusually high ECSA of 6958.33 cm^2, confirming that performance enhancement arises from genuine increases in accessible active sites rather than superficial current amplification. This is an important reminder of a major gap in the current state of knowledge where accurate normalization metrics are absolutely essential for comparison.

The enhanced catalytic efficacy is again demonstrated by its high exchange current density (j_0), obtained from the low charge-transfer resistance. A higher j_0 represents a reduced activation energy and rapid equilibration of reaction rates, directly correlating interfacial electronic properties to macro-scale reaction rates. Herein, CNTs and Mo–P/CNTs decoration *via* Mo–P synergistic bonding mitigates kinetic constraints by stabilizing reaction intermediates and, at the same time, enables efficient electron injection into interfacial orbitals, an effect that escaped previous phosphide-based electrocatalysis. In practice, j_0 is employed as an authentic indicator to validate

Table 4 Comparative values of R_s, R_{ct}, ECSA and J_o for prepared electro-catalyst

Electrocatalyst	R_s (ohm)	R_{ct} (ohm)	ECSA (cm^2)	J_o (mA cm^{-2})
MoP	4.2	3.78	2500	6.79
MoP/CNTs (10 mg)	0.035	3.58	2875	7.17
MoP/CNTs (15 mg)	0.0172	2.35	5541.667	10.92
MoP/CNTs (20 mg)	0.015	2.11	6958.33	12.16

the fundamental catalytic activity of different electrocatalysts, unaffected by transport limitations, as indicated by eqn (8). In particular, it can be obtained by fitting into the Tafel equation or EIS analysis. This improvement is largely owing to the superior electrical conductivity of CNTs, as depicted in Table 4, which enhances charge transfer by lowering charge-transfer resistance. Moreover, MoP/CNTs enhance interfacial interaction, overcome activation barriers, and enable facile charge transport, thus leading to superior catalytic activity.

$$J_o = \frac{RT}{n\,FR_{ct}} \tag{8}$$

where J_o is exchange current density, R ideal gas constant, F is Faraday's constant (96 485 C mol^{-1}), R is the universal gas constant (8.314 J mol^{-1} K^{-1}), n is the number of electrons transported, T is the absolute temperature (K), and R_{ct} is the charge transfer resistance.

The electrocatalytic durability of MoP/CNTs (20 mg) was quantitatively measured by chronopotentiometry and subsequent polarization analysis. As shown in Fig. 8(a), MoP/CNTs demonstrates a remarkably stable operation process during a prolonged current-driven electrolysis process over a period of 24 h with a very slight potential shift of only about 20–25 mV at a fixed current density. In addition to plotting a polarization curve, a linear sweep voltammetry (LSV) experiment was conducted to measure how well MoP/CNTs maintains its electrocatalytic activity. Fig. 8(b), presents negligible $\Delta\eta = 15$–20 mV at a current density of 10 mA cm^{-2} with a performance retention more than 95%.

The excellent stability can be attributed to the synergistic effect between MoP and the conductive CNTs framework. The CNTs scaffold ensures a mechanically stable and electrically conductive matrix, which is capable of tolerating the volume expansion occurring during the repeated redox cycles and thus prevents reduction of the catalyst. As a result, the efficiency of the charge transfer and accessibility to the active sites are retained during the electrolysis process. In summary, the above findings clearly demonstrate the excellent stability of the MoP/CNTs hybrid for electrocatalysis applications.

The HER kinetics help identify the critical key for assessing the practical merits of interfacial engineering in phosphide carbon interfaces. As revealed in Fig. 9, without optimization, the natural kinetics for MoP are quite low (50.9 mol_{H_2} g_{cat}^{-1} s^{-1}), thereby identifying an important underlying issue with unmodified transition-metal phosphide electrocatalysts: namely, that although favorable from an energetic standpoint for hydrogen adsorption, their actual activity is compromised by poor charge transfer and nanoparticle agglomeration during actual use.

Incorporation of the CNTs into the MoP system in an ordered manner causes a dramatic and monotonically increasing improvement in the hydrogen evolution reaction rate, with the rate increasing to 53.0, 71.2, and 79.3 mol_{H_2} g_{cat}^{-1} s^{-1} with the addition of 10, 15, and 20 mg of the CNTs, respectively. This behavior indicates more than the increase of electrical conductivity and the onset of the transition from the isolated catalytic regions to the percolated catalytic network with the coherent electron transport through CNTs, while the latter inhibit the agglomeration of the MoP particles, maintain the catalytically active edge regions, and provide the continuous pathways for electron transport between the catalytic regions

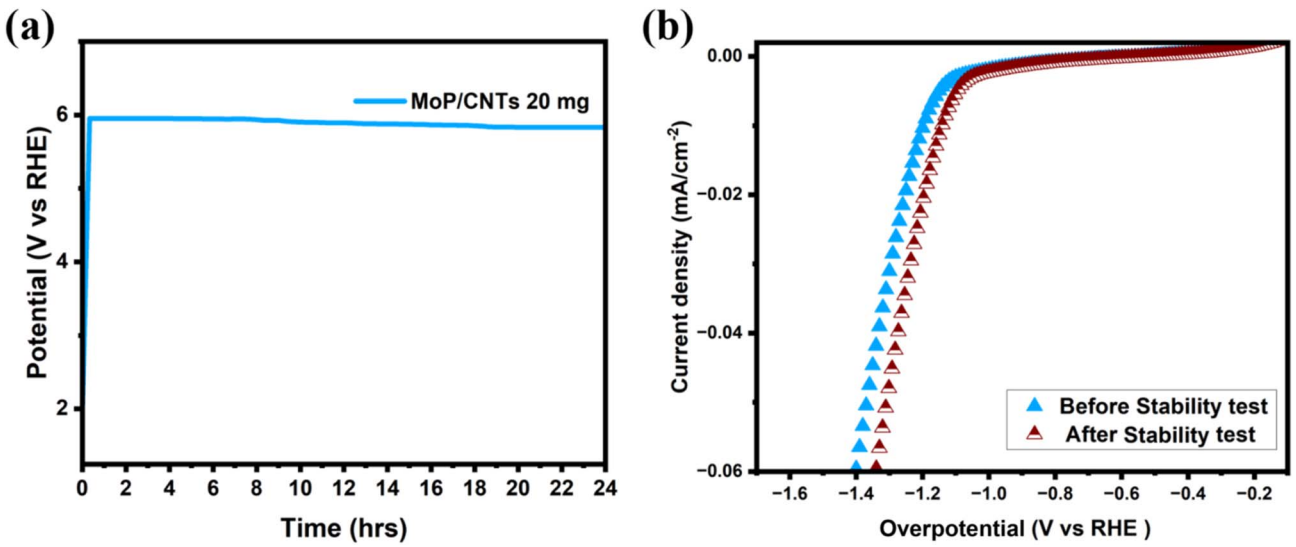

Fig. 8 Electrochemical stability of the MoP/CNT (20 mg) catalyst: (a) chronopotentiometric stability test and (b) LSV curves before and after durability testing.

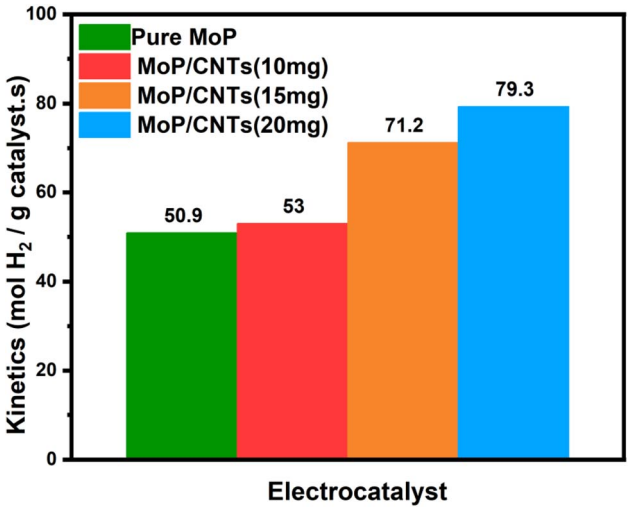

Fig. 9 HER kinetics for synthesized electro-catalyst.

and the current collector directly. This leads to the kinetically accessible electron supply to the hydrogen adsorbates.[51] Notably, these results resolve the paradox of previous phosphide catalyst designs, which have largely failed because enhancement through nanostructuring alone quickly becomes undermined by structural coarsening and interfacial barriers. Conversely, the MoP/CNTs heterostructure shows that kinetic acceleration and structural robustness have to be optimally balanced at the interface level to enable sustained activity. The fact that the kinetic acceleration with increasing amounts of CNTs shows the presence of an optimal concentration of conductive support beyond which increased transport becomes deteriorated because of site blocking again points to the need for compositionally optimized catalyst design. The kinetic equations derived in this work (extended in SI) have the potential to facilitate benchmarking, which still represents an area of need within the entire scientific community.

5. Proposed mechanism for water splitting

The electrocatalytic properties of the MoP/CNTs hybrid are dominated by the interfacial electronic interactions between the MoP nanodomains and the conductive CNTs matrix, and not by the individual atomic reaction steps as in the case of a traditional water-splitting catalyst. The strong MoP–CNTs interface leads to charge redistribution in the heterointerface, in turn altering the Mo and P electronic structures and the consequent adsorption energies in the catalyst–electrolyte interface.

In the alkaline HER process, the MoP/CNTs hybrid system favors the Volmer–Tafel reaction path, as evidenced by the experimental Tafel slopes, which remains small. The density of interfacial states at the MoP–CNT interface enables fast electron injection from the CNT to the MoP sites, thus reducing the activation barrier for the Volmer reaction ($H_2O + e^- \rightarrow H^* + OH^-$). In the proposed hybrid design, phosphorus regions work as preferred sites for the activation of

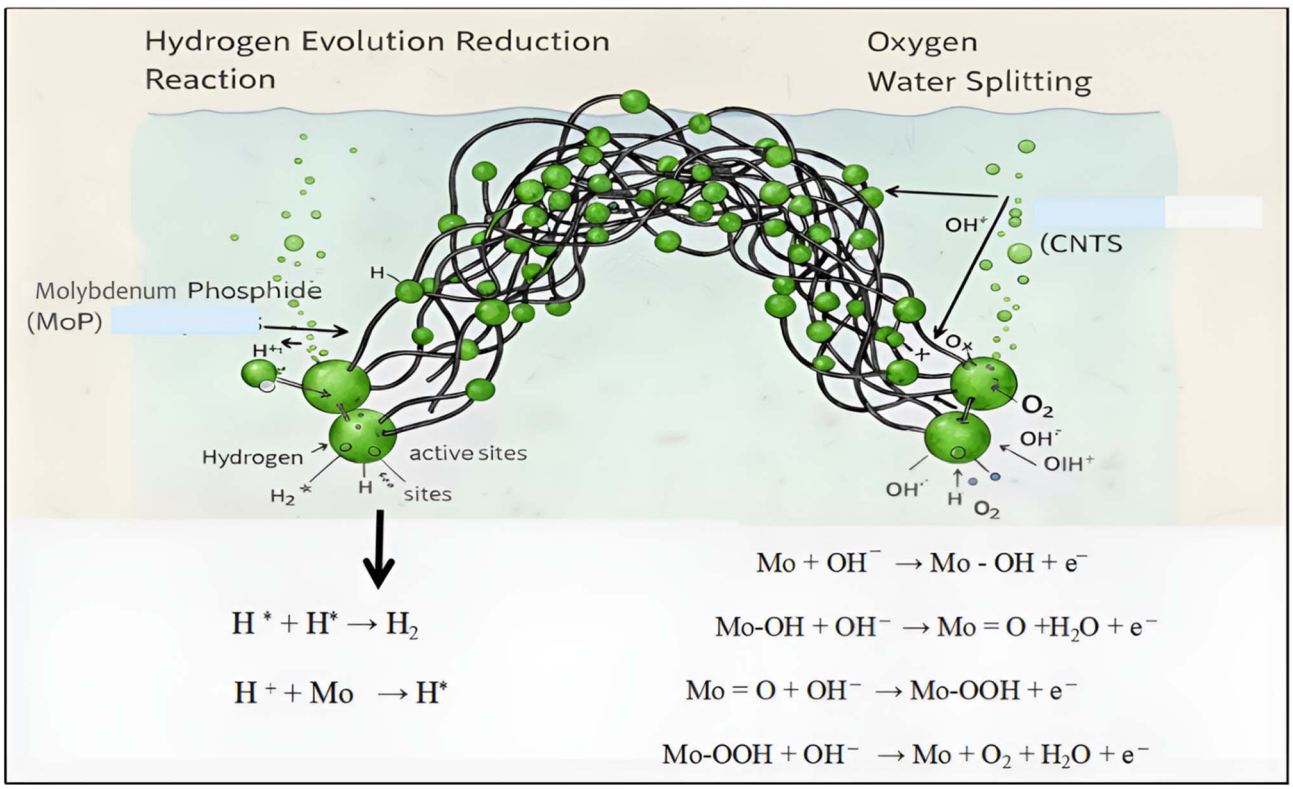

Fig. 10 Proposed mechanism for HER & OER in water splitting.

H2O, and the neighboring Mo areas have the strongest binding affinity for H* species. The CNTs scaffold provides an efficient reservoir for electrons and thus prevents the accumulation of charges at the MoP surface and allows for an increased surface concentration of H* species. This is followed by the Tafel recombination step ($H^* + H^* \rightarrow H_2$), thus allowing for faster HER kinetics compared to MoP due to slower charge transport in the latter.[52] During OER, the MoP/CNTs hybrid experiences electrochemically assisted surface reconstruction under anodic polarization, giving rise to Mo-related oxyhydroxide catalytic sites. Indeed, the CNTs scaffold retains uninterrupted charge transfer channels during the entire multielectron process of OER. The interfacial interaction between Mo-related surface reconstruction sites and the CNTs scaffold facilitates stabilized key intermediates, namely MoOHO*, MoO*, and MoOOH*, while resisting polarization losses that could be incurred during their generation as a result of interfacial interaction between Mo-related reconstruction sites and the carbon scaffold, as a carbon scaffold resists over-surface passivation by precluding electro-insulative oxide-layer deposition, thus supporting sustained OER activity when operated in alkaline medium conditions.

In summary, the promoted bifunctionality of MoP/CNTs hybrids can be attributed to the interfacial synergy, in which the regulation of electronic structure, facilitated charge transport, and surface reconstructions work together to control the reaction rates. The suggested mechanisms for HER and OER are shown in Fig. 10.

6. Conclusions

The current study focuses on an important issue related to the synthesis of non-noble metal electrocatalysts and the harmonious combination of high catalytic activity, fast charge transfer rates, and high durability under operation. Despite widespread concern about the excellent H adsorption properties, earth abundance, and excellent chemical stability of molybdenum phosphide (MoP), the substance has remained less explored as an electrocatalyst owing to the low conductivity and reduced effective surface area under the agglomeration of MoP. This study, which combines MoP nanoparticles with a conductive CNTs framework, strongly suggests the significant impact of the MoP–CNTs interface, instead of the MoP composition itself, in determining the efficiency of the electrocatalyst. The MoP–CNTs hybrid with an optimal amount of MoP (20 mg) shows superior electrocatalytic activity for the HER process with low overpotential of 81 mV at the current density of 10 mA cm^2, low Tafel constant of 34 mV dec^{-1}, and strong OER activity with low overpotential of 245 mV at the current density of 10 mA cm^2.

Furthermore, the long-term electrochemical stability experiments exhibit that the CNTs serve not only as conducting fillers, but also as the mechanistic and chemical support structures to retard the sintering process of the nanoparticles and the degradation of the interfacial regions when the cell is operated under alkaline environments. However, the time-evolution of the interfacial status of the Mo–P/CNTs interfaces when operating under the current density as needed by the industrial applications and its contribution to the long-term degradation and efficiency losses are still not understood. Furthermore, any practical translation of the current lab-scale-based research to industrial applications would require the precise control of the final electrode structure. To conclude, it appears that MoP/CNTs hybrids are still a general, adaptable catalytic system rather than any one optimized composition. The adherence to standardized benchmarking practices, involving measures of activity corrected for ECSA, high current density tests, and efficiency tests, will be critical to facilitate comparison between different studies, hence facilitating the adoption of phosphide-based electrocatalysts in industry.

Conflicts of interest

The authors don't have any conflict of interests that may have influenced the work in this research.

Abbreviations

MoP	Molybdenum phosphide
CNTs	Carbon nanotubes
HER	Hydrogen evolution reaction
OER	Oxygen evolution reaction
NPs	Nanoparticles
XRD	X-ray diffraction
SEM	Scanning electron microscopy
CV	Cyclic voltammetry
LSV	Linear sweep voltammetry

Data availability

All the research carried out in this work is original, produced by authors at School of Chemical & Materials Engineering (SCME), NUST, Pakistan. Data for this work can be made available upon request.

Supplementary information (SI) is available. See DOI: https://doi.org/10.1039/d6na00046k.

Acknowledgements

We would like to thank the Department of Chemical Engineering, SCME, NUST, Islamabad, Pakistan, for their support in this work. The NUST administration is also gratefully acknowledged for the provision of the lab facilities.

References

1 R. S. Nada, M. Emam and H. Hassan, *J. Phys.: Conf. Ser.*, 2024, **2857**, 012016.
2 D. Yang, W. Hou, Y. Lu, X. Wang, W. Zhang and Y. Chen, *ACS Sustain. Chem. Eng.*, 2019, **7**, 13031–13040.
3 R. Khosa, E. Pervaiz, U. Abdullah, M. Ali, U. Sohail and A. Shakoor, *Mol. Catal.*, 2022, **528**, 112514.
4 H.-M. Yang and Z.-Y. Yuan, in *Transition Metal-Based Electrocatalysts: Applications in Green Hydrogen Production*

and Storage, American Chemical Society, 2023, ch. 1, vol. 1435, pp. 1–20.
5 X. Xu, H. Liang, G. Tang, Y. Hong, Y. Xie, Z. Qi, B. Xu and Z. Wang, *Nanoscale Adv.*, 2019, **1**, 177–183.
6 R. Rajalakshmi, G. Srividhya, C. Viswanathan and N. Ponpandian, *Appl. Catal., B*, 2023, **339**, 123089.
7 Y. Jiao, Y. Zheng, M. Jaroniec and S. Z. Qiao, *Chem. Soc. Rev.*, 2015, **44**, 2060–2086.
8 A. Rodríguez-Gómez, F. Dorado, P. Sánchez and A. R. de la Osa, *J. Energy Chem.*, 2022, **70**, 394–406.
9 M.-R. Gao, J.-X. Liang, Y.-R. Zheng, Y.-F. Xu, J. Jiang, Q. Gao, J. Li and S.-H. Yu, *Nat. Commun.*, 2015, **6**, 5982.
10 J. Rongé, T. Dobbelaere, L. Henderick, M. M. Minjauw, S. P. Sree, J. Dendooven, J. A. Martens and C. Detavernier, *Nanoscale Adv.*, 2019, **1**, 4166–4172.
11 Q. Feng, L. Zeng, J. Xu, Z. Zhang, z. Zhiliang, Y. Wang, X.-Z. Yuan, H. Li and H. Wang, *J. Power Sources*, 2019, **438**, 227048.
12 C. Liu, X. Cao, L. Chen, Q. Wang, B. Zhang, C. Liang, Y. M. Lam and L. Wang, *ACS Catal.*, 2025, **15**, 14983–14995.
13 Y. Shi and B. Zhang, *Chem. Soc. Rev.*, 2016, **45**, 1529–1541.
14 B. Yu, L. Fei, L. Chen, Z. Dong, J. Chen, B. Guo, L. Zhou and Z. Ma, *J. Alloys Compd.*, 2025, 180729.
15 O. Siddiqui and I. Dincer, *Energy Fuels*, 2021, **35**, 670–689.
16 Q. Zhou, J. Feng, X. Peng, L. Zhong and R. Sun, *J. Energy Chem.*, 2019, **45**, 510–518.
17 M. F. Kaya, M. Kıstı, B. Hüner and N. Demir, in *Transition Metal-Based Electrocatalysts: Applications in Green Hydrogen Production and Storage*, American Chemical Society, 2023, ch. 9, vol. 1435, pp. 219–248.
18 Y. Wang, D. Zhang, Y. Yang, Y. Guo, Z. Bai, P. K. Chu and Y. Luo, *J. Alloys Compd.*, 2021, **872**, 159608.
19 S. Niknazar, A. A. Ensafi, E. Heydari-Soureshjani and B. Rezaei, *Chemosphere*, 2022, **294**, 133670.
20 A. Adam, M. H. Suliman, H. Dafalla, A. R. Al-Arfaj, M. N. Siddiqui and M. Qamar, *ACS Sustain. Chem. Eng.*, 2018, **6**, 11414–11423.
21 S. Karki, A. Mondal, A. Sinhamahapatra and P. G. Ingole, in *Transition Metal-Based Electrocatalysts: Applications in Green Hydrogen Production and Storage*, American Chemical Society, 2023, ch. 7, vol. 1435, pp. 169–203.
22 S. Khan, S. S. Shah, N. K. Janjua, A. B. Yurtcan, M. T. Nazir, K. M. Katubi and N. S. Alsaiari, *Chemosphere*, 2023, **315**, 137659.
23 Y. Jia, C. Zhang, H. Zheng, G. Zhang and S. Zhang, *Chemosphere*, 2024, **351**, 141195.
24 Z. Li, X. Dai, K. Du, Y. Ma, M. Liu, H. Sun, X. Ma and X. Zhang, *J. Phys. Chem. C*, 2016, **120**, 1478–1487.
25 C. Cheng, S. Zong, J. Shi, F. Xue, Y. Zhang, X. Guan, B. Zheng, J. Deng and L. Guo, *Appl. Catal., B*, 2020, **265**, 118620.
26 R. Khan, M. T. Mehran, M. M. Baig, B. Sarfraz, S. R. Naqvi, M. B. K. Niazi, M. Z. Khan and A. H. Khoja, *Fuel*, 2021, **285**, 119174.
27 M. Usman, D. Li, R. Razzaq, U. Latif, O. Muraza, Z. H. Yamani, B. A. Al-Maythalony, C. Li and S. Zhang, *J. Environ. Chem. Eng.*, 2018, **6**, 4525–4530.
28 S. Lefrant, M. Baibarac and I. Baltog, *J. Mater. Chem.*, 2009, **19**, 5690–5704.
29 D. Song, L. Wang, M. Yao, W. Sun, R. Vajtai, P. M. Ajayan and Y. Wang, *Adv. Sustainable Syst.*, 2020, **4**, 2000227.
30 J.-S. Li, X.-R. Wang, J.-Y. Li, S. Zhang, J.-Q. Sha, G.-D. Liu and B. Tang, *Carbon*, 2018, **139**, 234–240.
31 H. Jiang, L. Yan, S. Zhang, Y. Zhao, X. Yang, Y. Wang, J. Shen, X. Zhao and L. Wang, *Nano-Micro Lett.*, 2021, **13**, 215.
32 X. Li, X. Hao, A. Abudula and G. Guan, *J. Mater. Chem. A*, 2016, **4**, 11973–12000.
33 H. Du, R.-M. Kong, X. Guo, F. Qu and J. Li, *Nanoscale*, 2018, **10**, 21617–21624.
34 D. Kim, H. Nam, Y.-H. Cho, B. C. Yeo, S.-H. Cho, J.-P. Ahn, K.-Y. Lee, S. Y. Lee and S. S. Han, *ACS Catal.*, 2019, **9**, 8702–8711.
35 Y. Pei, Y. Cheng, J. Chen, W. Smith, P. Dong, P. M. Ajayan, M. Ye and J. Shen, *J. Mater. Chem. A*, 2018, **6**, 23220–23243.
36 C.-S. Yin, Y. Leng, X. Yang, C.-G. Min and A.-M. Ren, *Appl. Surf. Sci.*, 2024, **643**, 158605.
37 X. Zhang, X. Yu, L. Zhang, F. Zhou, Y. Liang and R. Wang, *Adv. Funct. Mater.*, 2018, **28**, 1706523.
38 X. Huang, X. Wang, P. Jiang, K. Lan, J. Qin, L. Gong, K. Wang, M. Yang, L. Ma and R. Li, *Inorg. Chem. Front.*, 2019, **6**, 1482–1489.
39 C. Huang, C. Pi, X. Zhang, K. Ding, P. Qin, J. Fu, X. Peng, B. Gao, P. K. Chu and K. Huo, *Small*, 2018, **14**, 1800667.
40 X. Li, J. Zhang, C. Zhang, D. Chen, B. Wang, R. Zhang, Y. Zhang, X. Yan, Q. Gan, S. Wang, H. Q. Luo and N. B. Li, *J. Solid State Chem.*, 2020, **290**, 121564.
41 S.-S. Liu, L.-J. Ma and J.-S. Li, *J. Colloid Interface Sci.*, 2023, **631**, 147–153.
42 Y. Gao, Z. Chen, Y. Zhao, W. Yu, X. Jiang, M. He, Z. Li, T. Ma, Z. Wu and L. Wang, *Appl. Catal., B*, 2022, **303**, 120879.
43 L. Lin, M. Chen and L. Wu, *Mater. Chem. Front.*, 2021, **5**, 375–385.
44 K. Ahanjan, M. Shamsipur, A. Taherpour and A. Pashabadi, *Electrochim. Acta*, 2022, **433**, 141249.
45 D. C. Nguyen, D. T. Tran, T. L. Luyen Doan, N. H. Kim and J. H. Lee, *Chem. Mater.*, 2019, **31**, 2892–2904.
46 M. R. Kandel, U. N. Pan, D. R. Paudel, P. P. Dhakal, N. H. Kim and J. H. Lee, *Composites, Part B*, 2022, **239**, 109992.
47 A. Wang, X. Chen, L. Cheng, X. Shen, W. Zhu, L. Li and J. Pang, *J. Mater. Chem. A*, 2020, **8**, 17621–17633.
48 P. Connor, J. Schuch, B. Kaiser and W. Jaegermann, *Zeitschrift für Physikalische Chemie*, 2020, **234**, 979–994.
49 T. Kawawaki, Y. Negishi and H. Kawasaki, *Nanoscale Adv.*, 2020, **2**, 17–36.
50 J. Li, J. Li, J. Hu and P. Chen, *Energy Fuels*, 2023, **37**, 17803–17835.
51 S. Deka, M. K. Jaiswal, M. P. Nath and B. Choudhury, *Water Splitting: Production of Hydrogen*, 2025, pp. 23–48.
52 T. Shinagawa, A. T. Garcia-Esparza and K. Takanabe, *Sci. Rep.*, 2015, **5**, 13801.